



# Reflectometry diagnostics for atmospheric entry applications: state-of-the-art and new developments

R. Grosso Ferreira<sup>1</sup> · J. Vicente<sup>1</sup> · F. Silva<sup>1</sup> · B. Gonçalves<sup>1</sup> · L. Cupido<sup>2</sup> · M. Lino da Silva<sup>1</sup>

Received: 21 July 2022 / Revised: 12 January 2023 / Accepted: 13 January 2023 / Published online: 4 February 2023  
© The Author(s) 2023

## Abstract

Insight into the plasma properties of high-speed ionized flows is key for the validation of predictive aerothermodynamic tools for atmospheric entry applications, namely plasma radiation which will be highly dependent on the flow electron densities, which accordingly need to be accurately estimated. We performed an extensive review on past re-entry microwave diagnostics, including both in-flight and ground-test experiments. This work assesses the peculiar characteristics of entry plasmas, and derives functional requirements for microwave diagnostics tailored for such applications. A preliminary analysis, including a simulation of electromagnetic environment for the RAM-C II flight experiment, obtained through a CFD code coupled to an electromagnetic propagation code, is presented. The obtained results outline the adequacy of such diagnostics for improving verification and validation for high-speed entry plasma flows.

**Keywords** Atmospheric entry · Electron density · Plasma · Reflectometry · Interferometry

**Mathematics Subject Classification** 76L05 · 76K05 · 76X05

## 1 Introduction

Electron density is one of the keys for the comprehension and understanding of every kind of plasma, and this includes atmospheric entry plasmas. Although these have typically low ionization degrees (around  $10^{-4}$ – $10^{-2}$ ), electrons still play an important role in the kinetic and radiative processes of these high-speed, reactive flows, namely through electron-impact excitation reactions. The electron density also affects communications blackout, and therefore, influences the positioning of communication antennas. Finally, knowledge of the spatial distribution of electron densities is relevant for the validation of aerothermodynamic codes deployed for the prediction of the aerodynamic forces and thermal heat fluxes sustained by an entry spacecraft.

Historically, electrostatic (Langmuir) probes are relatively simple diagnostics that have been successfully deployed for the measurement of such electron densities and temperatures [1], however they suffer from a few drawbacks, the most important being that these are intrusive diagnostics that perturb the flow in the measurement region. An alternative is to use non-intrusive techniques such as microwave interferometry/reflectometry.

Microwave reflectometry is a radar-like technique mostly based on the dispersive properties of the medium where waves propagate. The technique was originally employed to measure the ionospheric structure [2, 3] and found a large range of applications in fusion plasma diagnostics following a rapid development in the mid-1980s [4–6]. Reflectometry is well suited for measurements of both equilibrium and fluctuating components of several plasma parameters, such as the electron density. A review of several microwave-based techniques for plasma diagnostics can be found in [7]. A comprehensive description of reflectometry fundamentals can be found in [1] while a review of the technique can be found in [8]. An overview of present-day diagnostic systems and capabilities is found in [9]. In particular, the electron density profile can be reconstructed if electromagnetic waves are reflected in the plasma where a cutoff condition is met.

✉ R. Grosso Ferreira  
ricardojoaogmferreira@tecnico.ulisboa.pt

<sup>1</sup> Instituto de Plasmas e Fusão Nuclear, Instituto Superior Técnico, Universidade de Lisboa, Av. Rovisco Pais, 1049–001 Lisboa, Portugal

<sup>2</sup> LC Technologies, Rua da Vila Verde 39, Eixo, 3800–810 Aveiro, Portugal

Note that relativistic effects may appear for electron temperatures above 1 keV [10], however this is not the case for re-entry plasmas where the electrons are thermalized in the absence of external electromagnetic fields.

In short, microwave interferometry/reflectometry is a mature technology that is routinely deployed in many fusion reactors all around the world. Surprisingly, this technology is yet far from mainstream for atmospheric entry applications, despite a few successful in-flight experiments as far back as the 1960s and the deployment of this technique in ground test facilities dedicated to atmospheric entry plasmas. The objective of this work is to present this state-of-the-art and provide the specifications and requirements for an electron density microwave diagnostic tailored for atmospheric entry applications (both in-flight and ground-testing).

This work is organized as follows: Sect. 2 presents the state of the art on experimental reflectometry experiments with an emphasis for space applications, with a description of in-flight experiments and deployments in ground-test facilities; Sect. 3 outlines the specifications and requirements for the design of a reflectometer/interferometer suited for atmospheric entry applications, focusing on the electron densities of interest. These may vary by several orders of magnitude, depending on the entry speeds (orbital or super-orbital), or whether the spacecraft forebody shock layer or afterbody expansion flow is probed. A coupled CFD/wave propagation simulation has been carried out for the well-known RAM-C flight experiment which successfully deployed this measurement technique in the 1960s, showcasing the electromagnetic wave propagation dynamics. Finally Sect. 4 presents the concluding remarks, and the perspectives for atmospheric entry applications of this technique.

## 2 State of the art

### 2.1 First principles

A probing signal  $S_{src} = A_{src} \cos(\omega t)$  is sent to the plasma via a waveguide/antenna, it propagates until a layer with refraction index  $N(\mathbf{x})$  equals zero is found, where it reflects. The received signal  $S_{rcv} = A_{rcv} \cos(\omega t + \phi)$  differs with respect to  $S_{src}$  in both amplitude and phase  $\phi$ . The phase is decomposed as  $\phi = \phi_u + \phi_0 + \phi_p$ , which represent the propagation in the waveguide, vacuum and plasma, respectively. The waveguide phase can be known through calibration, the vacuum phase is easily estimated, finally, plasma information can be inquired from the last term. The refraction index can be related to the electron density  $n_e(\mathbf{x})$  through the Altar-Appleton equation [11]. Particular relevance for the hypersonic atmospheric re-entries is the so-called O-mode, where a wave's electric field is parallel to the exterior/imposed magnetic field or when the latter is non-existent. For O-mode propagation,  $\phi_p$

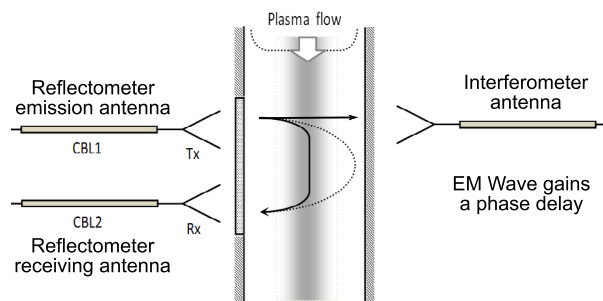


**Fig. 1** Differences between the reflectometer and interferometer methodology to probe electron density of a plasma

is a function of the wave's vacuum frequency  $f$  and of the refractive index  $N(\mathbf{x})$ , where the latter depends only on the electron density, and collisions between electrons and heavy particles are neglected, thus  $\phi_p[f, N(n_e)]$ . In practical terms, two configurations may be used to probe the electron density of a plasma: Reflectometer and interferometer.

Figure 1 shows the differences between the two methods. In reflectometry the EM wave reflects when encountering a region whose electron density is above a critical value  $n_c$ . By performing a frequency sweep covering the relevant range of critical electron density values, the spatial electron density profile can be drawn out. The selected probing frequencies must be around the cutoff frequency for the expected peak electron density. In interferometry, an EM wave with frequency higher than the plasma cutoff frequency, passes through the plasma gaining a phase delay compared to the vacuum, from which an average electron density can be calculated. Since this is an integrated signal, it must be post-processed to create a real plasma profile, via Abel-inversion or “onion-peel” techniques. The chosen frequencies should be well above the critical  $n_c$  to prevent unwanted reflections. Both techniques can be used in mono- or bistatic configurations, in the first configuration one antenna is used for both emitting and receiving the EM waves, in the latter, emission and reception each are performed by a dedicated antenna. For the case of monostatic interferometry the probe signal reflects at the wall, so the wave passes through the plasma twice, and these phase delays must be taken into account. In bistatic reflectometry the emitted EM wave “hits” the plasma at an angle, so a second antenna is required for the reception. This phenomena may also occur due to the plasma profile refractive index, which may not reflect the EM wave back to the emitting antenna.

The complex plasma-wave interactions in turbulent media have driven the continuous development of both analytical theory and sophisticated full-wave numerical codes to support the interpretation of reflectometry data. Typical analytical solutions require simplifications and approximations of the plasma parameters. Figure 2 compares a laminar to a

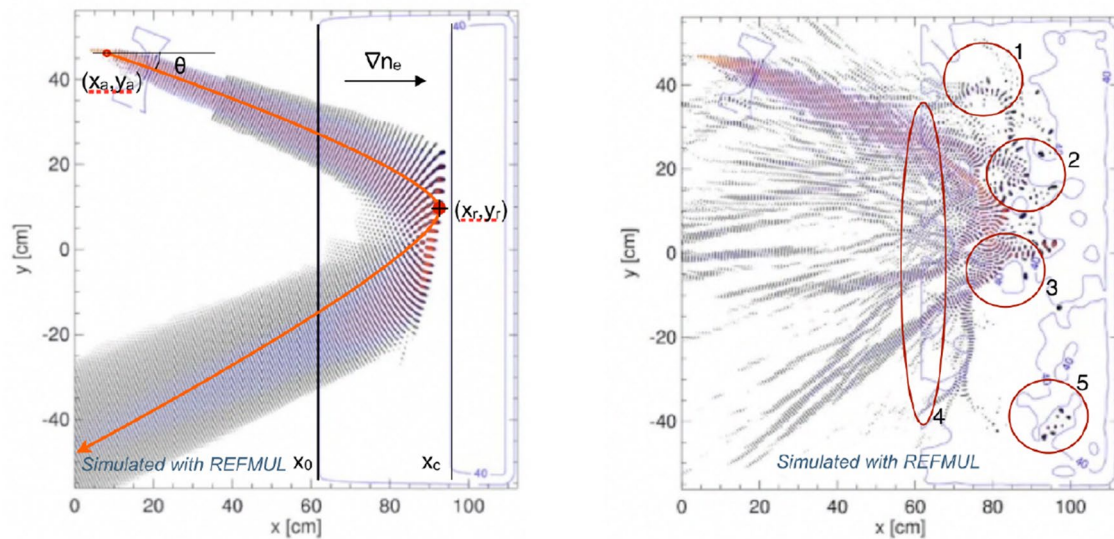


**Fig. 2** Simulation with REFNUM for a non-turbulent plasma (left) and a turbulent plasma (right), taken from F. Silva in [13]

turbulent plasma. Turbulence can originate effects such as: multi-scattering; local resonances; secondary cutoffs; beam splitting and 5-wave trapping. These will scatter the emitted EM waves, lowering the received power and difficult the signal interpretation. A fullwave numerical code may be required to properly design and validate a reflectometer. In this work, to overcome many shortcomings of the analytical descriptions while modeling any real sized geometry, the two-dimensional finite-difference time-domain (FDTD) full-wave code REFNUM [12] is used to simulate wave propagation while retaining fundamental physics, as described in detail below.

### 2.1.1 Specific challenges for entry applications

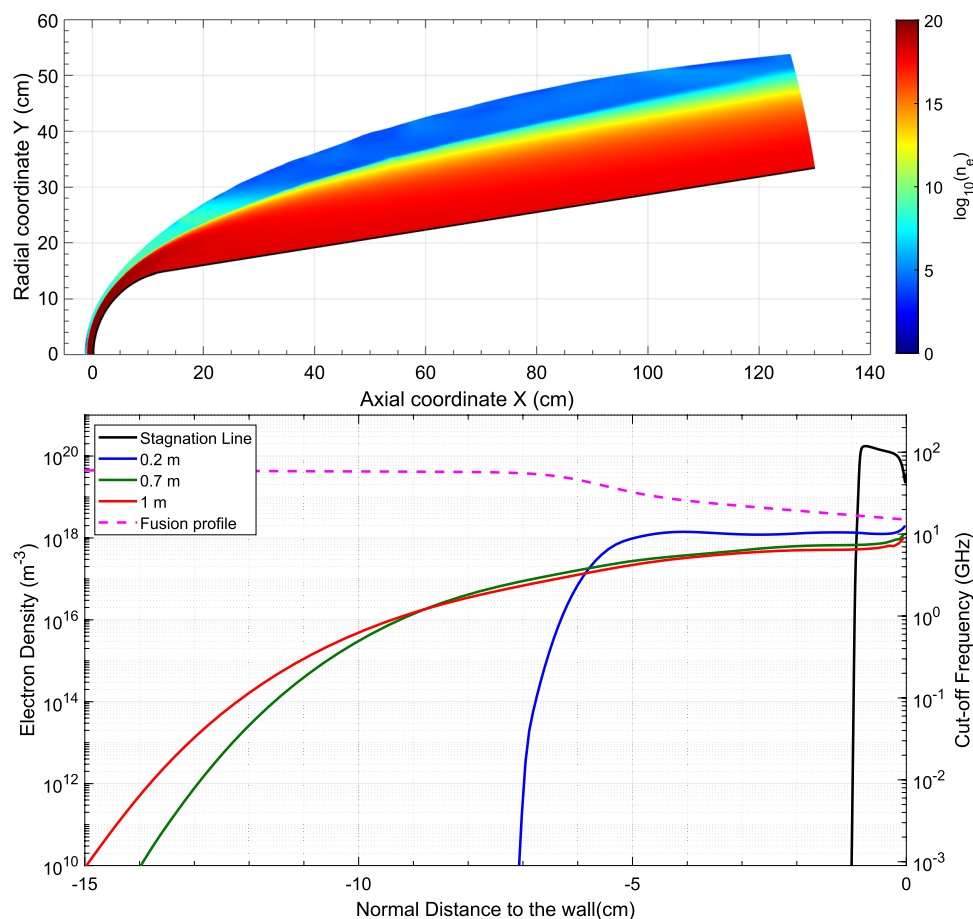
It is important to properly address the specific features of entry plasmas, compared to larger scale plasmas, such as in fusion applications. The usual electron density profile of a fusion plasma has a positive gradient towards the center, a radial like profile. This means that the plasma has a low electron density near the reactor walls and antenna position, and high electron density at the center. Such trend is helpful in creating a density profile, since as the probing signal frequency increases, so does the reflection point distance. An easy density *vs.* distance profile may be drafted from the reflectometer data, as the device sweeps the plasma at different frequencies and collects the reflected signal.

This is not so for atmospheric entry plasmas that typically showcase a relatively steep gradient at the boundary layer, with a decrease of density away from the spacecraft wall. As an illustration, we present in Fig. 3 a simulation of the RAM-C II flight experiment which has been simulated

within our group in the recent past [14]. In the stagnation-line region, we have a shock-wave lying very close to the spacecraft surface (1 cm), with a peak electron density in the shock-layer, and a steep decrease in the boundary layer, owing to catalytic wall recombination reactions. In the flow wake, the shock-standoff distance is up to 15 cm, with much lower densities in the post-shock region where flow velocities increase to supersonic conditions. This leads to a higher global density gradient towards the boundary layer, and we may even witness an increase of electron densities near the wall, despite losses from catalytic recombination. Such density profile accordingly becomes “counter-intuitive” to typical reflectometer applications where the antenna is closer to the lower density side. This limits the capability for tracing the electron density profile beyond the first peak, since a full profile cannot be obtained, as the reflectometer is essentially “blind” beyond the higher electron density peak. A more detailed discussion on the RAM-C II testcase will be presented in Sect. 2.2.1.

A further problem arises from the typical dimensions of atmospheric entry plasmas. Most vehicles have dimensions which are lower than those of larger tokamaks, namely the vehicles for robotic exploration which may be less than 1 m in diameter. Only larger man-rated vehicles such as the Space shuttle or larger capsules have sizes significantly larger than most tokamaks. Additionally, the plasma flow is severely constricted between the bow shockwave and spacecraft surface, with a thin shock and boundary layer lying very close to the wall, and a larger plume in the wake. This means that typical shock standoff lengths may be in the order of the cm, compared with the characteristic lengths of the larger tokamaks, which may exceed 1 m. Such small

**Fig. 3** Top: Navier–Stokes simulation for RAM-C, Electron density at 61 km altitude. Bottom: Electron density profiles normal to the wall at the antennas location and stagnation line. A typical electron density profile from a tokamak fusion plasma is added for comparison purposes, from [16]. The RAM-C II simulations data is taken from [14]



scales yield a few problems of their own: The probe signal is reflected very shortly after the antenna exit, which hinders a reliable measurement, and the plasma length scale is similar to the reflection layer, meaning an accurate reflection position cannot be inferred. The smaller spacecraft scales further induce a few other practical issues: reflectometer needs to be light and compact since weight and volume are a premium in space missions, and commonly used horn antennas may also be too large to be easily integrated in a spacecraft and there is the further risk of destruction due to direct contact with the plasma [15].

Last but not least, typical electron densities differ among both applications. Typical electron densities range between  $10^{17}$ – $10^{21}$  el./m<sup>3</sup> in tokamaks, and  $10^{16}$ – $10^{22}$  el./m<sup>3</sup> in atmospheric entry flows. This means that different frequency bands will be relevant for each application, and the spatial accuracy will also differ (since it depends on a first approach on the wavelength of the corresponding frequency bands).

## 2.2 Inflight experiments

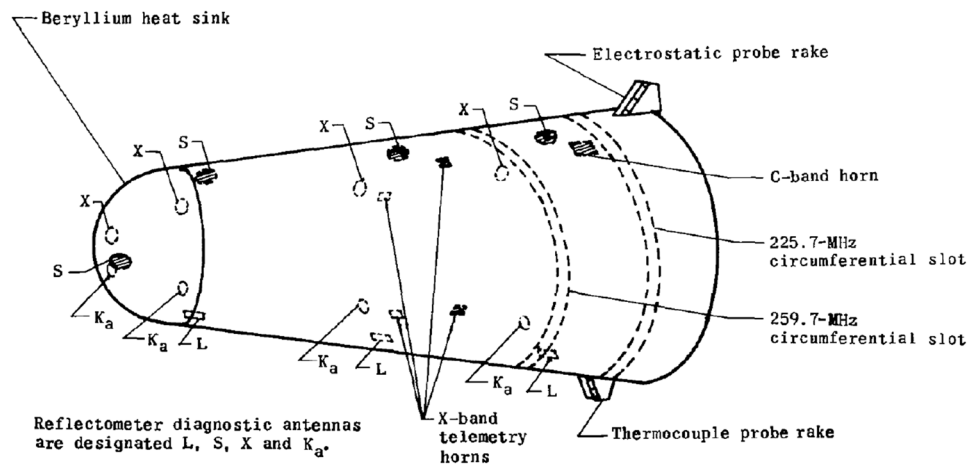
To date, a total of five in-flight experiments with *in situ* of the electron density/temperature measurements were designed over the last 60 years. These include, in chronological order,

the RAM program in the 60's and MRIS in 1989 by NASA, OREX and HYFLEX in 1994 and 1996 by JAXA and ARD in 1998 by ESA. The RAM program ran between 1960 and 1970, MRIS was halted during the engineering phase.

### 2.2.1 RAM-C II

The “Radio Attenuation Measurements” (RAM) program was designed by the NASA Langley Research Center and U.S Department of Defence. The motivation of this program was to increase the understanding of blackout phenomena and finding ways to minimize resulting in-flight problems [17]. Since calculations for the aft (rear) plasma profile require knowledge of the gas history as well as local chemistry, from the shock entry point to the aft point, the RAM program was also designed to validate and help improving computational models and the understanding of plasma formation in both nose and aft body regions. The program was comprised of a theoretical and an experimental part, the latter with tests in ground facilities followed by in-flight experiments (RAM C). Three flight experiments were performed with a hemisphere-cone body at a velocity of 7620 m/s to measure plasma parameters and

**Fig. 4** RAM C-II reflectometer antennas positions, adapted from [17]



test radio-attenuation alleviation techniques. Only the second flight (RAM C-II) was equipped with a reflectometer.

**2.2.1.1 Reflectometer equipment** Four-stage solid-fuel Scout vehicles were used to launch RAM C-II body up to an apogee greater than 220.5 km, then propelling it back into Earth's atmosphere. The spacecraft was spin-stabilized prior to the motor ignition reentering with a nominal flight-angle path of  $-15^\circ$ , reaching a maximum velocity of 7678 m/s at 67.0 km of altitude. The payload geometry was approximately 15 cm (6-in.) radius hemispherical nose followed by a  $9^\circ$  half-angle cone and had an overall length of about 130 cm (51-in.). The payload had a teflon afterbody and a beryllium heat sink nose cap, with a mass before the launch of 121.8 kg. The beryllium-cap and teflon body were found not to release significant amounts of alkaline impurities, fulfilling its propose of avoiding contamination so the measurements could be compared with pure-air models. All RAM C flights had negatively biased Langmuir probes, that will not be discussed here.

A four-frequency microwave reflectometer was put into the RAM C-II payload to infer the peak electron density time and altitude history. The antennas are positioned along the body as shown in Fig. 4. The radiofrequency of the NATO L-, S-, X- and  $K_a$ -bands correspond to 1,116, 3,344, 10,044 and 35,000 MHz, respectively.

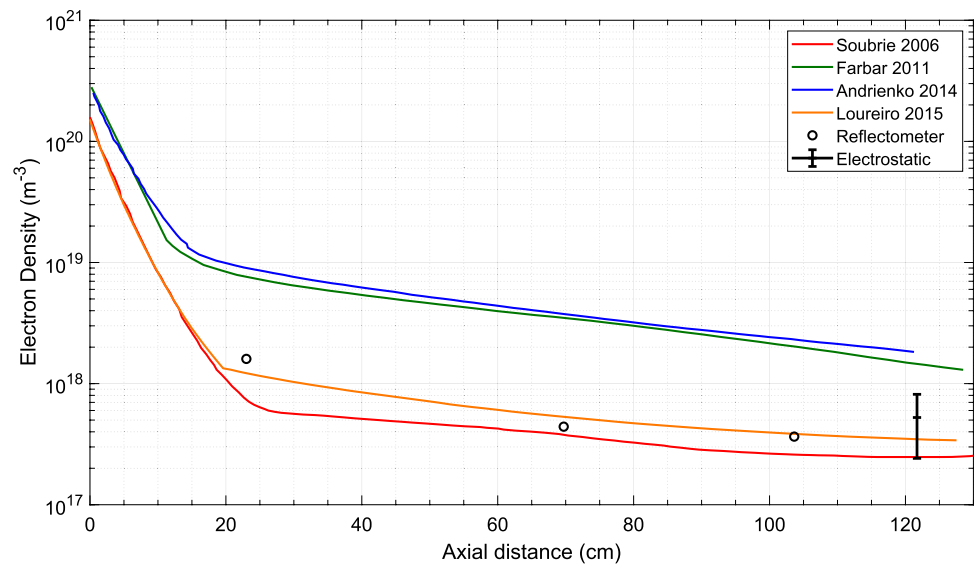
Each reflectometer system was composed of a microwave signal source, an isolator, a four-way power divider (three-way for L-band) to split the signal into the various antennas, bidirectional couplers, four electric field probes, and antennas. Open-end waveguides were used as antennas for the nose region, where plasma reflective layer distance to the surface was small. On the aft region X- and  $K_a$ -bands used high gain horn-antennas and L- and S-bands used open waveguides.

**2.2.1.2 Mission outcomes** The electron density measurements from the reflectometer antennas had good agreement with the ones from Langmuir probes. A strong density gradient was observed between payload surface and the flow for the first 1–2 cm. After that, the density value is stable for several centimetres. The plasma density showed a strong correlation with the longitudinal position [17].

The numerical simulations were done using a clean-air assumption. This was considered valid down to 56.4 km, whereas in the case of RAM C-I flight the flow was by then contaminated by ablation products [17]. Reflectometer data was more accurate than electric probes data as the latter were influenced by the temperature around them. For a valid interpretation of the fixed-bias electric probes an accurate knowledge of the leading-edge temperature is required. Above 1366 K (measured by the thermocouple) the insulating properties of the dielectric were degraded. Thus, the validity of the data interpretation was questionable. For lower altitudes, the comparison between experimental reflectometer data and computation calculations are invalid, as pointed in [18]. The reasons are the higher neutral-electron collision frequency and the ablation of microwave antennas. This ablation changes short-circuit-phase reference and introduces a small voltage standing wave ratio which complicates data interpretation. The sharp rise in reflection coefficient is not as sharp due to neutral-electron collision frequency and thus a clean signal of the reflective layer is no longer visible.

The plasma at the aft body region, measured over the 7 cm deep electrostatic probe rake, was larger and less dense than expected [18]. A reasonably good agreement between experiment and computational model was found for the electron density gradient in the nose region. This agreement was not observed for altitudes higher than 70 km. The electron density was consistently higher in the computational model,

**Fig. 5** RAM C-II electron wall density. Comparisons between measurements and numerical simulations from different authors (Soubrié 2006 [21]; Farbar 2011 [20]; Andrienko 2014 [19] and Loureiro 2015 [14])



this over-prediction means that at the aft region the electron density will also be over predicted. The author also reports that free electrons are originated from ionization in the nose region, and then move to the aft body. A possible reason for the deviation between computational and experimental data at the rear may be the lack of implementation of ambipolar transport in the numerical code. Over the years, the RAM-C experiment has become a popular CFD validation test-case experiment, with many authors (including us [14]) using its data to validate and improve the kinetic models of numerical codes [14, 19–21], study the catalicity effects on the electron density [20, 22] or the ambipolar diffusion effects of ions [23]. As attested in Fig. 5, good reproduction of these past experimental results is nowadays achieved by contemporary CFD models in this lower speed orbital entry regime. More details on our CFD model [14] will be presented in section 3.2.1.

### 2.2.2 OREX and HYFLEX

The Japanese space agency (JAXA) performed studies and experiments during the development of the H-II Transfer Vehicle (HTV), [24]. To study the re-entry conditions of said vehicle, two flight experiments were designed and launched, the Orbital Re-entry Experiment (OREX) and the Hypersonic Flight Experiment (HYFLEX).

OREX was a half-cone sphere capsule equipped with Langmuir probes to evaluate electron density and TPS in a flight environment [25, 26]. The flight took place in February 1994, with results showing good agreement with CFD simulations, see Gupta et al. [26].

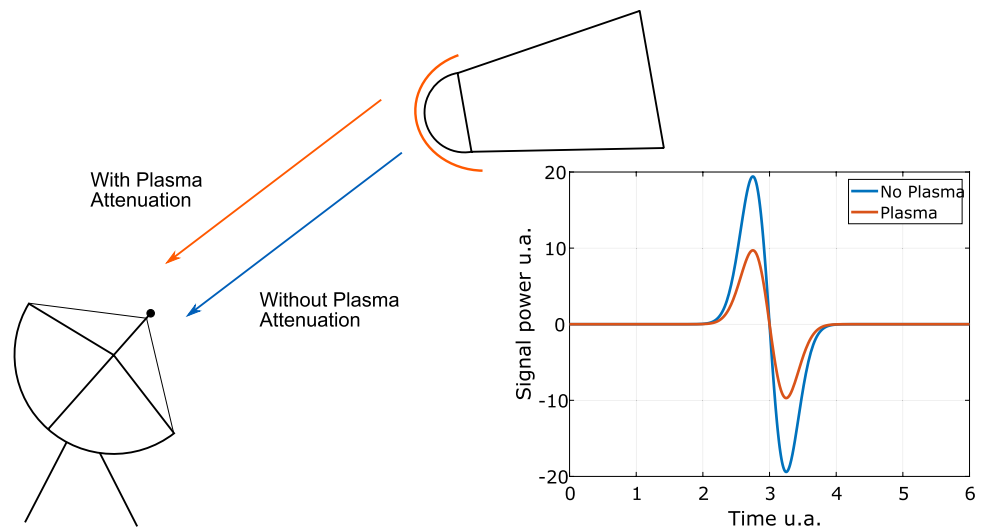
The HYFLEX vehicle had a slender lifting-body design, more complex than the OREX capsule. Its objectives included the validation of the aerodynamic design, data

acquisition, and the evaluation of the aerothermodynamic properties of the vehicle. For the latter objective HYFLEX was equipped with temperature and pressure sensors, as well as two reflectometers [24, 27]. The maximum electron density predicted for the re-entry was around  $10^{17}$  el./m<sup>3</sup>. The reflectometers center frequency was set to around 1 GHz to account for the plasma layer being thinner than the wavelength. The selected frequencies were 902.85 and 1676.5 MHz, with the antennas installed 960 mm aft from the nose of the ship and 180 mm off center. These were rectangular waveguides with 135x267 mm and 74x145 mm, respectively. In these locations, the aluminium skin of the ship was replaced with a Kevlar panel and thermal protection tiles were attached to it. The panel and tile effect on the reflectometer waves was found to be negligible, as reported in [27].

The reflectometer system was comprised of an oscillator, circulator, detector, amplifier, and a standing wave ratio (SWR) section for the 902.85 MHz only. The radio wave generated from the oscillator traveled through the circulator into the antenna. The EM wave was then reflected at the plasma and entered via the same antenna to the circulator. It was lastly received at the detector, where the reflected wave intensity was measured. The SWR section function was to measure the phase of reflected wave, which was useful for inferring the distance from the antenna to the plasma layer. Unfortunately, the data quality was not enough to be useful.

Flight data from the reflectometers was analysed via the power reflection coefficient. The expected reflection coefficient was estimated using a numerical simulation, then compared to a ground test using a metallic plate. Good agreement was observed between the 3D simulation and the ground test. The flight reflectometry data showed agreement in shape and peak values with the CFD simulations,

**Fig. 6** Illustration of communications attenuation during re-entry



nonetheless the peak occurred sooner than expected. The high frequency signal (1676.5 MHz) showed a power reflection coefficient peak of 0.2, whereas for the low frequency (902.85 MHz) a peak coefficient of 0.3 was found. This dependence is reasonable, since the lower frequency wave should be reflected in an easier fashion than the higher one. The blackout time and duration is consistent with the observed VHF telemetry data from the ground station. The obtained results found a peak electron density of  $10^{17}$  el./m<sup>3</sup>, for a plasma thickness of about 1 cm. Using the VHF telemetry attenuation signal, the plasma density around the antenna was compared to the CFD simulation with good agreement of peak plasma density of  $10^{15}$  el./m<sup>3</sup> and thickness of 50 cm.

### 2.2.3 Atmospheric reentry demonstrator—ARD

The Atmospheric Reentry Demonstrator (ARD) was a ESA flight mission with multiple objectives, among these, the testing and validation of re-entry technologies and flight-control algorithms, qualification of design and TPS, study of radio communications and black-out, and validation of aerothermodynamic predictions during re-entry [28]. The ARD shape was a 70% scale Apollo capsule, with a diameter of 2.8 m and weight of 2.8 tonne. Two reflectometer antennas were located 45° off the center axis in the leeward side of the heat shield, and the working frequencies were 2.203 and 2.218 GHz respectively [29]. The reflectometers were comprised of a power unit and a waveguide, and were calibrated against a metallic target pre-flight, and then again post-flight. Results differ between the two calibrations, and are in agreement with each other only at altitudes below 45 km. Above 97 km, the post-flight calibration gives slightly higher peak electron densities around  $7.75 \times 10^{16}$  el./m<sup>3</sup> vs.  $1.24 \times 10^{16}$  el./m<sup>3</sup> at 45 km. However, between the 90–45 km altitude

the post-flight values do not converge to a valid solution. The pre-flight calibration gives a peak electron density of  $1.52 \times 10^{17}$  el./m<sup>3</sup>. The authors of [29] argue that the reason for the different calibration results may be related to the plasma formation and the corresponding metallic plate erosion in the antenna region.

### 2.2.4 Other radio attenuation measurements

Several works have examined the attenuation of VHF and UHF telemetry radio waves during spacecraft entries to assess the electron densities in the flow. Typical approaches imply simulating the CFD flowfield (and particularly the plasma density profile) at different reentry times and overlaying an electromagnetic solver to determine the signal attenuation for specific paths over the plasma. Then a comparison of the real attenuation (signal telemetry before/during reentry) is carried out. While this does not allow for fine estimations of the flow density, it is sufficient for a coarse estimation of the CFD reconstruction accuracy, namely comparing the rate of change for the electron densities along the different trajectory points. An illustration of this is shown in Fig. 6. Examples of such works may be found in [30, 31] for ESA's Inflatable Re-Entry Technologies (IRDT) and [32] on ARD.

ESA's IRDT mission communication operated in UHF band with frequency of 219 MHz mounted in the nose of the capsule. During re-entry communications blackout only lasted 45 s instead of the expected 80 s. Reynier et al [30, 31] reconstructed the electron density profile, then used a EM solver to simulate the observed attenuation at different frequencies. Their results predicted a signal attenuation ranging from –6 to –15 dB at different frequencies. The initial 1D engineering estimation using the plasma critical density over-estimated the blackout time as observed in the flight.

Takahashi et al [32] used a similar methodology to study ARD's blackout of the Tracking and Data Relay Satellite (TDRS) communication at 2.267 GHz. The attenuation results at the rear was low enough to permit communications, except at 70 km altitude. However, Tran [29] reports that there was never a full blackout at TDRS band, despite a strong attenuation at 70 km. On the front side of ARD the blackout was complete.

### 2.2.5 Cancelled flight experiments

NASA's Microwave Reflectometer Ionization Sensor (MRIS) program, fully detailed in [33], began in 1989 to develop a millimetre wave reflectometer to evaluate the electron density during a hypersonic re-entry. The program was halted in 1991, with the design phase completed and the engineering model near completion. The instrument design was composed of 4 antennas operating at 20, 44, 95 and 140 GHz. The equipment is divided into two-parts, a detector and an emitter/receiver part. The 20 GHz frequency antenna works in a monostatic configuration, while the others in a bistatic configuration. The lower frequency limits were chosen due to the antenna size limitations, the upper limit was limited by device reliability and receiver sensitivity. The frequency sweep was chosen to have a bandwidth of 4 GHz using a conventional stepped-FMCW frequency modulation continuous wave (FMCW) linear approach. Vector Error Correction (VEC) was identified as a powerful tool to improved the performance of the equipment.

MRIS equipment radiates modulated millimetre wave (mmW) signal into the plasma field and then coherently detects the phase and amplitude of the reflected signal received in the antennas. This information is used to reconstruct the electron density, the amount of reflected power, and the distance up to the plasma reflective layer. This density is specific for each mmW, and the bands are narrow enough so that the signal delay time can be used to estimate the critical density distance.

The instrument specifications could be met at all frequency bands for targets further than two inches away without the need for any vector error correction. Nonetheless, the use of VEC improved the accuracy and was required in Band-C and Band-D to meet the requirements for target distances less than two inches. A more sophisticated detection algorithm was used in Band-C where a simple algorithm was insufficient.

## 2.3 Ground test facilities

Shock tubes and Plasma Wind Tunnels are used to reproduce typical conditions for entry plasmas for aerothermodynamics experiments. In such ground test facilities, reflectometry and interferometry equipments are used alongside spectroscopy

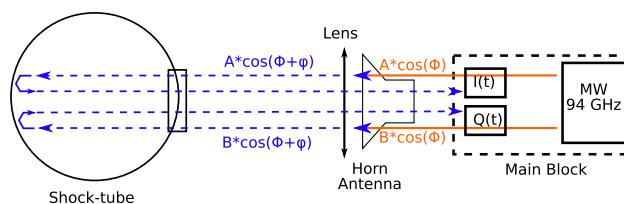


Fig. 7 MIPT shock tube 94 GHz microwave 2-Channel Interferometer

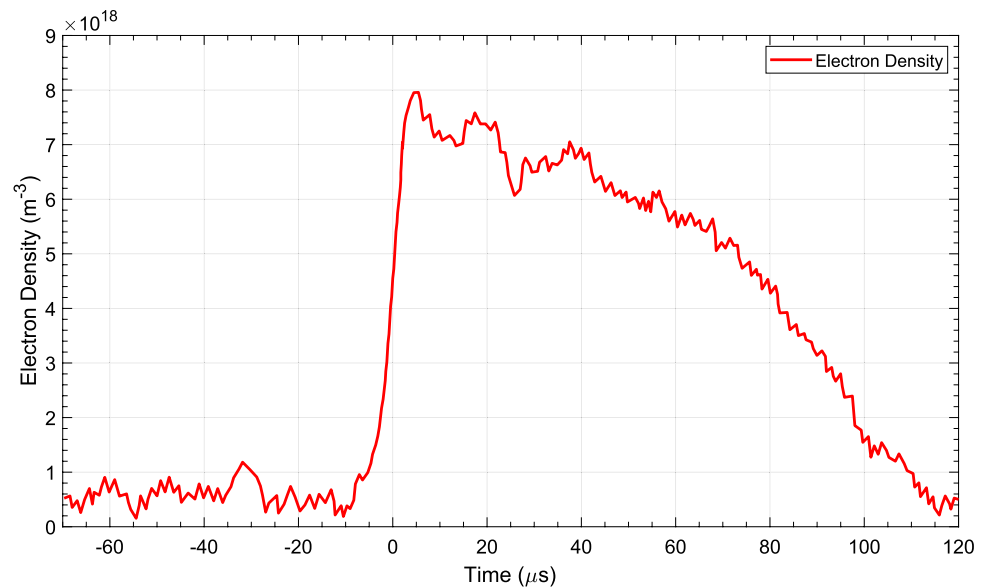
diagnostics. These have the advantage of measuring electron density directly. A series of experimental programs have been developed over the different decades for probing electron densities and temperatures, but have mostly been restricted to Langmuir probe techniques or indirect spectroscopic measurements, such as Stark-broadening measurements of the H- $\alpha$  atomic lines. Examples like these are too many and out of the scope of this work, and we will only review applications of the reflectometry/interferometry principle.

### 2.3.1 Shock tube interferometry measurements

An experimental campaign under the auspices of the European Space Agency (ESA) [34–38] has been carried out in 2008 at Moscow Institute of Physics and Technology (MIPT) shock tube. The campaign objective was to validate the existing CFD tools employed in the design of the EXOMARS mission. A two channel 94 GHz microwave interferometer was used to determine the electron density. It works combining two microwaves whose phases are  $\pi/2$  shifted. The microwave will gain a phase as it propagates in the plasma proportional to the electron density. The working frequency is selected to ensure that it will not reflect in the expected plasma conditions. Nonetheless, a posterior spectral analysis can confirm the results, and if the interferometer wave reflected at the wall or mid-away in the plasma. Figures 7 and 8 depicts a schematic of said interferometer and the measured electron density for a sample experimental shot in MIPT.

The interferometry principle can also be applied to combustion or shock tube experiments. A 94 GHz interferometer was used in a combustion shock tube [39] to measure the electron density of thermally ionized argon and krypton gases. Schneider et al [40] used a microwave interferometer to measure the ionization rates of NaCl-contaminated argon flames. Other authors [41–43] conducted similar experiments which will not be detailed here.

**Fig. 8** Measured electron density for a shockwave speed 3470 m/s, filling pressure 6.2 Torr (826.5 Pa), gas mixture CO<sub>2</sub>



### 2.3.2 Plasma plume reflectometry measurements

Interferometry/reflectometry are useful techniques for non-intrusive probing of the electron density of a plasma plume. Its main advantage is being non-intrusive contrary to the usual Langmuir probes [44, 45], however the acquired signal is a line integration over the density profile. To create the 2D or 3D density profile an inversion method to the line integrated signal must be applied. These can vary from a “onion-peel” or Abel-inversion to more complex techniques such as Tikhonov deconvolution, described in [46].

Several works have been done in characterising a plasma plume with microwave diagnostics. The electron number density of a closed drift SPT-100 Xenon Hall thruster was mapped by Ohler et al. [47, 48], with a discharge voltage and current of 300 V and 4.5 A. Using a 17 GHz microwave interferometer via differential phase measurements the thruster plume profile could be obtained. The same group also characterized a 1 kW hydrogen plume in [49].

Capelli et al in [50, 51] used a 90 GHz interferometer to probe the electron density of a 200 W Hall thruster. Using an Abel-inversion, they could reconstruct the electron density profile of said Hall thruster. Kuwabara et al. [52] studied the plasma density fluctuations of a 200 W class magnetic layer type Hall thruster. They used a 76 GHz interferometer to probe the electric field fluctuations. In 2021 Kuwabara et al [53] measured the electron density using the same 76 GHz interferometer.

In 2008 a swept Frequency Modulated Continuous Wave (FMCW) reflectometer for space plasmas was first designed to measure electron density in a space environment. The reflectometer swept frequencies in the range of 2–18 GHz, which corresponds to critical electron densities in the order of  $4.96 \times 10^{16}$  to  $4.02 \times 10^{18}$  el/m<sup>3</sup>. A full sweep could be

performed in less than 100 microseconds and signal acquired for up to 10 milliseconds at a time, or up to 100 sweeps. Spatial resolution was determined to be less than 1.5 cm using at 16 Megasamples per second and a spectral length of 1024 samples. The system could operate in both monostatic or bistatic configuration. A complete description of the equipment and the test can be found in [54]. A typical schematic for a reflectometer in monostatic configuration is depicted in Fig. 9.

In 2010, the equipment was tested in the Von–Karman Institute 1200 KW Induction Plasmatron. A shift in the wall reflection frequency was observed when the plasma was turned on, from 2.2 to 1.8 GHz. The FFT amplitude signal can be observed in Fig. 10. The shift represents the difference in the time of flight of the wave. The shift is towards a lower frequency, this corresponds to a slower wave, as it propagates in the plasma the EM wave is slowed down in comparison to the vacuum propagation. Conclusions from the test were positive as the system operated as anticipated and the results in agreement with the other Plasmatron diagnostics. A thorough report of this test is presented in [54].

## 3 Designing a compact reflectometer/interferometer for entry applications

Owing to the extensive legacy of in-flight experiments and ground testing results, it is somewhat surprising that such a diagnostic is not more widespread than it currently is with in the hypersonics research community with no deployed instrumentation of this kind existing to the authors knowledge. Despite being a very complete diagnostic, reflectometry has a number of challenges to overcome to be correctly implemented. First, it requires the equipment antennas to

**Fig. 9** Schematic of the reflectometer

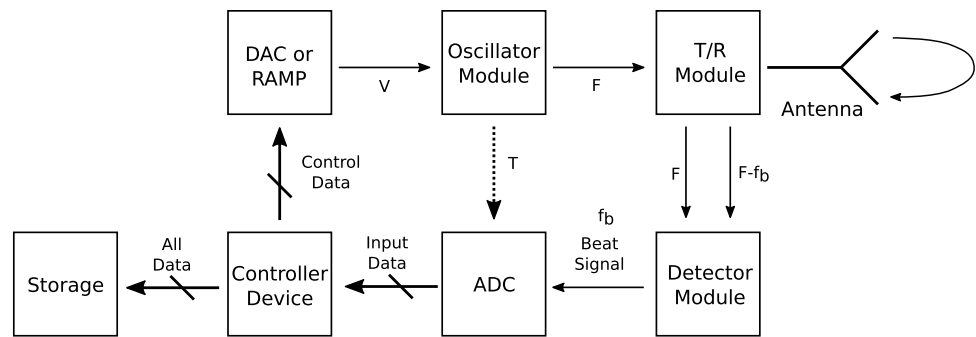
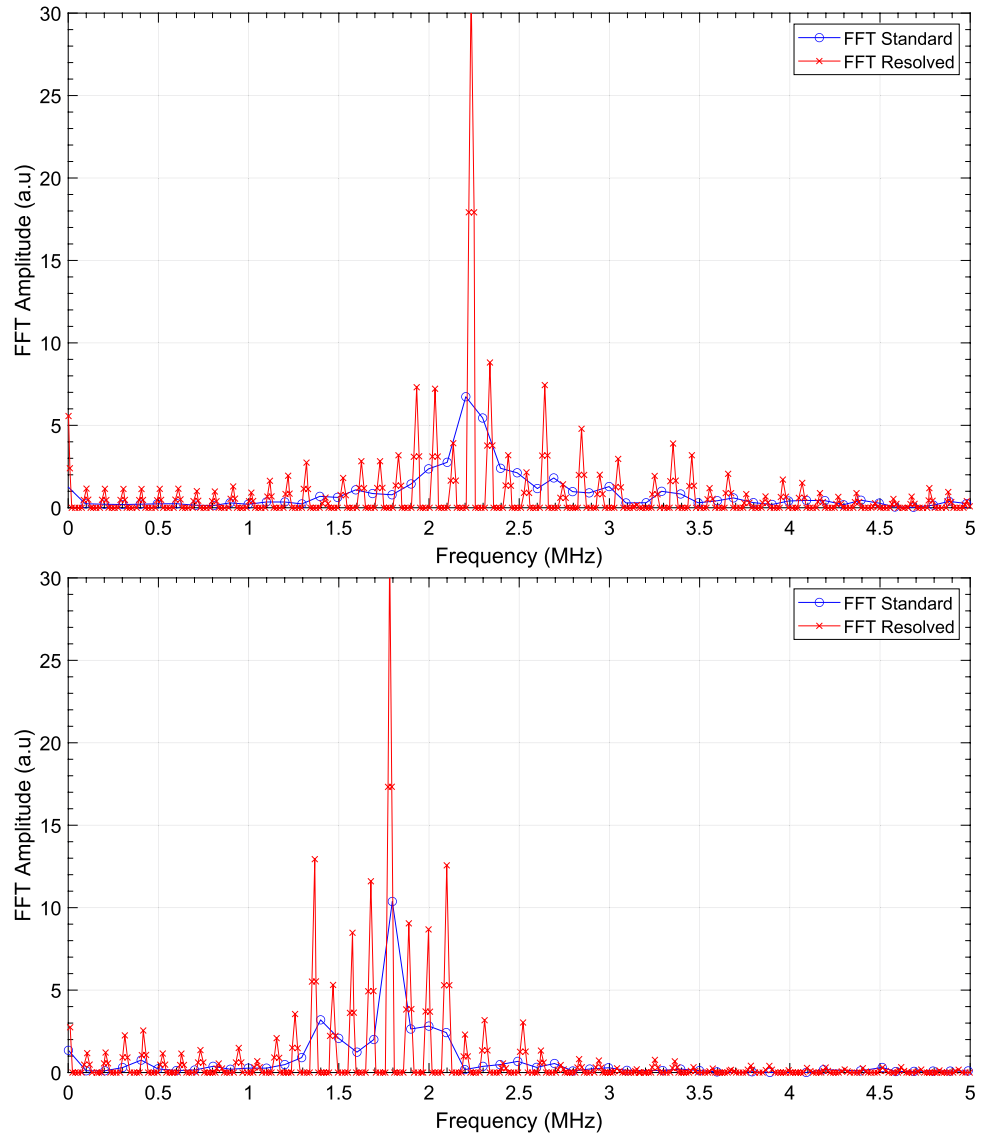


**Fig. 10** Wall reflection frequency testing at VKI plasmatron. Plasma turned off (top), plasma turned on (bottom), recreated from [54]



be directly exposed to hypersonic flow. These will be damaged during the re-entry and alter the received EM signal. Another limitation of this technique is the difficulty in interpreting the signal and relate it to the electron density value. The reason is the already mentioned steep electron profile

and small distance between the antenna and the plasma reflective layer. Besides it, the high electron density at the boundary layer further complicates the data interpretation. A pre-flight calibration of the reference levels can be used to help interpreting the reflected signal. For example,

microwave reflection coefficient was used by NASA in the RAM-C II [18] to identify the critical electron density by a steep rise in the reflected power. Nonetheless, this is a non-trivial technique and the used approximation may not be always valid. Communication blackout is no longer a prominent problem in spacecraft and lastly, these diagnostics are relatively heavy and cannot be simply added to a existing mission.

This is somewhat even more surprising as the knowledge of time/space resolved electron densities in atmospheric entry plasmas can enable a reliable quantitative assessment of key processes in such high-speed flows, as discussed in Sect. 1 (physical-chemical processes, flow history, blackout characteristics, and plasma radiation<sup>1</sup>).

### 3.1 Specifications and requirements

A reflectometer tailored for in-flight and ground test facilities is going to have a certain amount of limitations when compared to diagnostics tailored for fusion activities, see for example [55]. Mostly these are identical to other embarked diagnostics where one needs to ensure

- Compactness
- Low weight
- Low power consumption and good hibernation characteristics
- Adequacy to Space environment

For the last bullet point we may distinguish between flight experiments which target Earth re-entries, where the spacecraft remains inside Earth's magnetosphere from launch to touchdown (and where the overall mission may last hours instead of years), and other planetary entries, with a mission profile of several years where the spacecraft needs to withstand the cosmic environment. In this latter case one needs to define radiation-hardened or fault tolerant hardware, just like in fusion applications (owing to the severe radiation environment found in Tokamaks), however this discussion is beyond the scope of the paper, and the reader may refer to [56] for examples of radiation-tolerant hardware.

Naturally, these architecture requirements derive from the functional requirements of the setup. These include:

- Available frequency bands
- Frequency sweep characteristics
- High-speed remote control and acquisition
- Data storage and transmission

For the selection of appropriate frequency bands, one may firstly refer to the bibliographical review presented in Sect. 2. The operational frequencies for the RAM-C II experiment ranged between 1 and 35 GHz, whereas the HYFLEX and ARD experiments had reflectometers with frequencies in the 1–2 GHz range. These were tuned for measuring sparser electron densities, characteristic of the backbody plumes for these flight experiments. Freestream flow experiments in supersonic plasma wind tunnels, in the absence of an obstacle, will typically reproduce the conditions of these afterbody plasma plumes, and it is reasonable to consider similar frequencies. Hence a good candidate bandwidth would be in the 1–50 GHz to account for most of practical situations.

In contrast, electron densities in the stagnation region are predicted to be significantly higher, and although reflectometry experiments have limited viability in the stagnation streamline region, owing to the small shock standoff, one may nevertheless carry out interferometry experiments in shock tube facilities, such as the ones carried out in the VUT-1 shock tube. Here, the higher electron densities will mandate higher frequencies, above the plasma cutoff, and even for slower shocked flows around 3–4 km/s, a 94 GHz frequency was considered for the VUT-1 reflectometer. In the absence of other experimental data from shock tube facilities, it is then relevant to carry out numerical simulations of faster superorbital entry flows, to achieve an idea of the necessary interferometry frequencies in these more extreme flight regimes. Accordingly, we have simulated a 10 km/s shot from NASA's EAST shock tube, using our in-house SPARK CFD code. The obtained results are presented in Fig. 11 showing that the plasma cutoff frequency reaches a higher limit of about 2 THz. This means that interferometry diagnostics in shock tubes should be carried at very high frequencies, with a minimum of 100 GHz, and a maximum in the THz range (ideally 10 THz), otherwise the electromagnetic waves will not cross the plasma layer, rendering measurements unfeasible. However this does bring some additional challenges in terms of developing appropriate hardware.

### 3.2 Application to the RAM-C II test case

To further assess the behaviour of a compact reflectometer in the conditions of an atmospheric entry the RAM-C II flight experiment was modeled using a CFD (SPARK) code coupled to a wave propagation code (REFMUL). This allows achieving a better understanding on the propagation dynamics of the electromagnetic waves in an environment characteristic of an atmospheric entry, which in turn helps better tailoring the position of the reflectometer antennas, allowing precise measurements of the electron density profiles of the plasma.

<sup>1</sup> which is highly influenced by the plasma electron density.

**Fig. 11** SPARK 1D simulation results for Earth atmosphere at pressure of 0.2 Torr (26.66 Pa) and shockwave velocity of 10.29 km/s

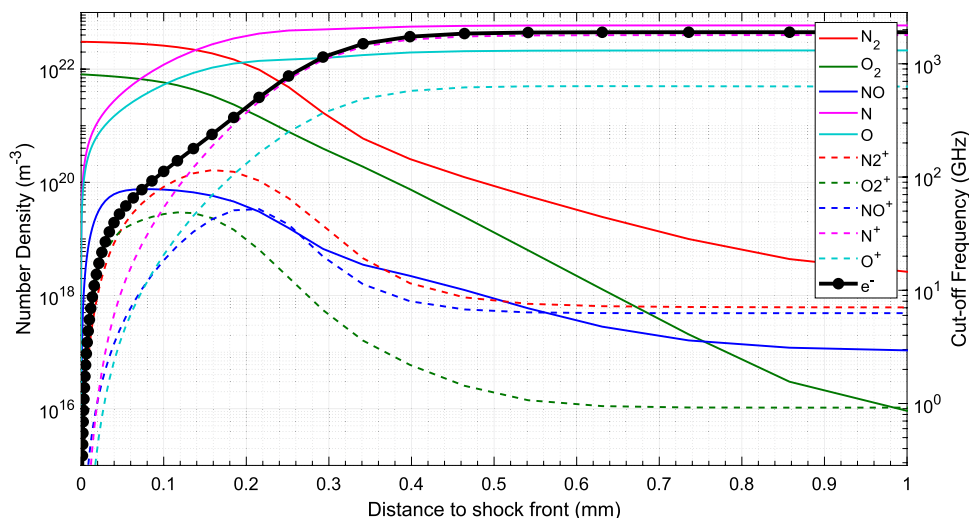


**Table 1** RAM-C II flight data, from [18], and peak electron density at stagnation line, from [14]. Shock stand-off distance  $\sim 2$  mm for all cases

| Time (s) | Altitude (km) | Velocity (km/s) | $n_e$ ( $\text{m}^{-3}$ ) | $f_{cut}$  |
|----------|---------------|-----------------|---------------------------|------------|
| 392.3    | 81            | 7.65            | $1.189 \times 10^{14}$    | 97.9 MHz   |
| 396.9    | 71            | 7.65            | $5.326 \times 10^{19}$    | 65.53 GHz  |
| 402.3    | 61            | 7.65            | $1.746 \times 10^{20}$    | 118.64 GHz |

The starting point is given by the critical conditions of the flight experiment (peak heating and peak dynamic pressure). These have been extensively discussed in the literature and will not be expounded here. The relevant flight points are outlined in Table 1.

Here we have chosen the 61 km altitude point and carried out a CFD simulation, followed by an overlay of the wave propagation code over the simulated plasma profiles. Section 3.2.1 and 3.2.2 provide an abridged description of the codes and models used in this simulation, then Sect. 3.2.3 presents the simulation results.

### 3.2.1 CFD code

The Software Package for Aerothermodynamics, Radiation and Kinetics (SPARK) is a computational fluid dynamics code designed for hypersonic reentry flows. It uses object-oriented programming to implement different physical models and numerical methods in a unified framework, which allows for greater flexibility and maintainability than other available numerical tools [57]. The code itself is capable of performing 0D (temporal relaxation), 1D (post-shock relaxation) or 2D (planar or axisymmetric) simulations using Navier–Stokes compressible flow-formulations for a nonequilibrium, multicomponent chemically reacting gas mixture. The code employs a cell-centered finite volume

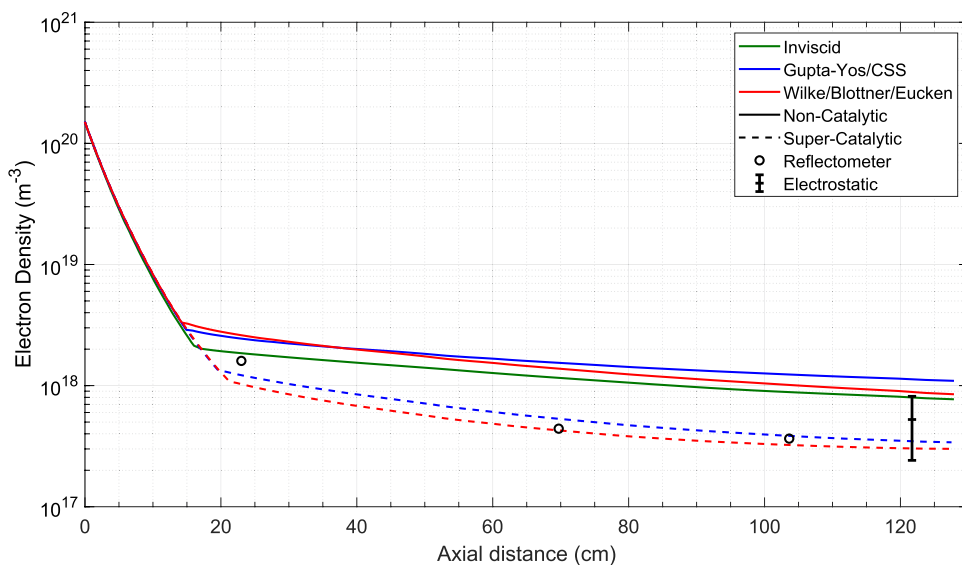
formulation, whereas, for the temporal discretization, both explicit (Roe) and explicit (Harten–Yee predictor-corrector) second order schemes are available. The nonequilibrium flow description accounts for separate global or individual vibrational temperatures, using a Millikan & White model coupled to a Park nonequilibrium chemistry model.

Simulations for the 61 km altitude have been carried out assuming a simplified 2D axi-symmetric geometry, with an  $80 \times 160$  mesh refined in the shock and boundary layer regions. Thermal and chemical nonequilibrium was assumed, for the following freestream conditions:  $v_\infty = 7.65$  km/s,  $T_\infty = 244$  K, and  $\rho_\infty = 2.73 \times 10^{-4}$  kg/m<sup>3</sup>. The 11 species ( $\text{N}_2$ ,  $\text{O}_2$ ,  $\text{NO}$ ,  $\text{N}$ ,  $\text{O}$ ,  $\text{N}_2^+$ ,  $\text{O}_2^+$ ,  $\text{NO}^+$ ,  $\text{N}^+$ ,  $\text{O}^+$ ,  $\text{e}^-$ ) 2001 Park chemistry model [58] was considered, and multi-component transport was treated either using the Wilke [59] or the Gupta–Yos [60] model. A non-catalytic/supercatalytic 1200 K wall was considered in two sets of simulations. Grid convergence was checked through a simulation using a mesh with double the size ( $160 \times 320$ ), which yielded similar wall fluxes results in the boundary layer. As seen in Fig. 12, the transport model has a slight influence on the electron properties at the wall, which is not surprising as the Wilke and Gupta–Yos models yield similar results for the lower temperatures associated to orbital entry velocities such as the one from RAM-C II [14]. Further, and as expected, the wall boundary conditions have a more marked influence on the simulated electron densities, with a supercatalytic boundary condition providing the best agreement with experimental data. This is a reasonable assumption, owing to the surface materials utilized in the RAM-C II experiment, see Sect. 2.2.1.

### 3.2.2 Wave propagation code

Full-wave codes are required in modelling wave propagation in order to retain the physics of several wave effects.

**Fig. 12** RAM C-II electron wall density. Comparisons between measurements and numerical simulations from different authors



This is the case for instance when the radiated fields of a specific antenna need to be simulated and/or small distances are considered which do not allow to work with far-field assumptions. The REFMUL\* codes family allows the simulation of reflectometry diagnostics coupling wave propagation, a time-dependent plasma, antennas positions and waveguides. The REFMUL\* family is a finite differences in time-domain (FDTD) unconditional stable algorithm using the Yee-scheme to discretize the spatial coordinates. The system of equations solved by REFMUL\* codes are the curl equations from Maxwell’s electromagnetism laws, coupled with a linear current density model. Currently there are four REFMUL\* codes, REFMUL, REFMULX, REFMULF and REFMUL3. The first three codes are already proven in simulating 2D waves, they simulate the O-mode, the X-mode and a generic wave polarization [12, 61–66], respectively. The REFMUL3 code is in advanced development phase and is capable of simulating a 3D full-wave. REFMUL\* system of equations to solve is the following:

$$\begin{cases} -\epsilon_0 \frac{\partial \vec{E}}{\partial t} + \vec{\nabla} \times \vec{H} = \vec{J} \\ +\mu_0 \frac{\partial \vec{H}}{\partial t} + \vec{\nabla} \times \vec{E} = 0 \\ \frac{\partial \vec{J}}{\partial t} = \epsilon_0 \omega_p^2 \vec{E} + \omega_c \frac{\vec{B}}{|\vec{B}|} \times \vec{J} \end{cases} \quad (1)$$

The plasma parameters are inserted in the equations through the plasma frequency  $\omega_p = \sqrt{e^2 n_e(\mathbf{x}) / m_e \epsilon_0}$ , the cyclotron frequency  $\omega_c = |eB(\mathbf{x}) / m_e|$  accounts for the external magnetic field.

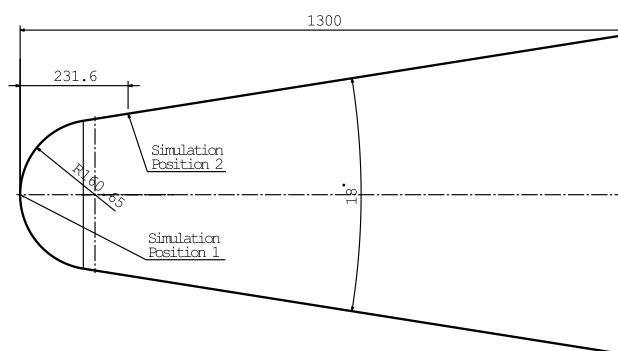


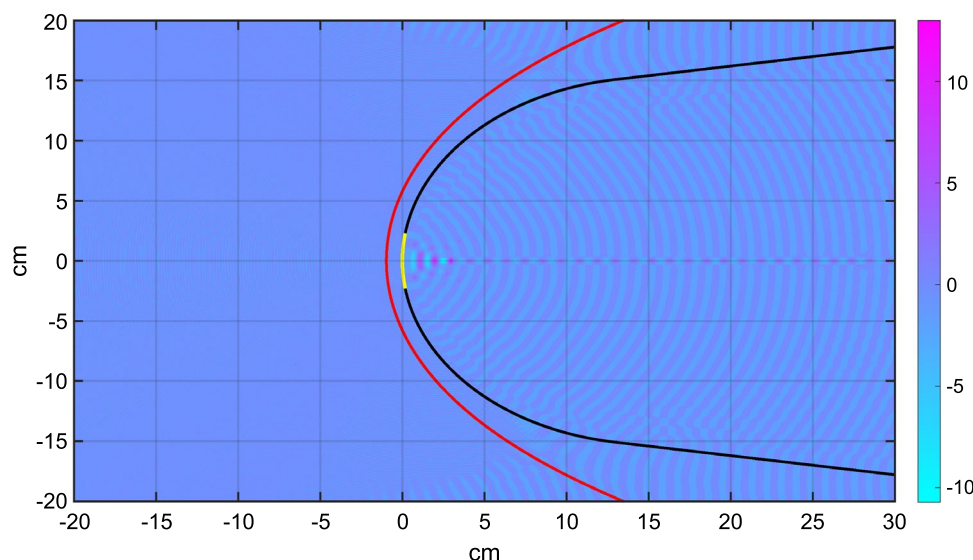
**Fig. 13** REFMUL simulation antenna positions, dimensions in mm

The response of O-mode reflectometry was studied using a monostatic design, i.e. one antenna for both emission and reception. A unidirectional transparent source was used for injection of the signal in a waveguide structure allowing separating the emitted probing wave from any returning waves [12]. A PML (Perfectly Matched Layer) approach was used for boundary conditions [67]. The spatial resolution of the Cartesian grid was  $\Delta x = \Delta y = \lambda(40 \text{ GHz}) / 20 = 3.75 \times 10^{-4} \text{ m}$ , where  $\lambda(40 \text{ GHz})$  is the vacuum wavelength of a wave with frequency in vacuum  $f = 40 \text{ GHz}$  which is an upper limit of the frequency range employed here. The time resolution of the REFMUL simulations was  $\Delta t = T(40 \text{ GHz}) / 40 = 6.25 \times 10^{-13} \text{ s}$ .

### 3.2.3 Results

The numerical simulations used antennas in positions similar to the RAM-C II experiment. Figure 13 depicts the antenna positions used in the numerical simulations. A first

**Fig. 14** REFMUL simulation in RAM-C II conditions, wave frequency 35 GHz. Spacecraft in black and shockwave in red. EM wave electric-field represented by the colorbar



simulation of reflectometry with a  $K_a$  band wave (35 GHz) in the RAM-C II nose region, position 1 in Fig. 13. The results are depicted in Fig. 14. The spacecraft outer wall is represented by the black line, the shockwave by the red line, the electric field in blue-purple colors. Preliminary simulations for the nose position showed that the emitted wave was reflected shortly after emission, as expected. The result shows a good integration between the SPARK CFD code and REFMUL EM wave code.

Another simulation was performed using a similar setup, but with the reflectometer antenna in the half-cone region, position 2 in Fig. 13, with results shown in Fig. 15. The EM wave propagates towards the shockwave, where a partial reflection of the wave occurs towards the rear occurs. Part of the emitted wave is deflected and passes the shockwave, and another is reflected back to the emitting antenna. In this position, the density profile peaks at a lower density and is further away from the outer wall. This improves the capability of reflectometry to provide a reliable density profile measurement in standard microwave frequency ranges.

These kind of simulations are useful for determining the propagation dynamics of the emitted electromagnetic waves, and the variability that stems from the emitted wave frequencies, but also from the electron density profiles in the flow. This allows better tailoring flight experiments, where one may consider developing standard reflectometry techniques, based on the time-of-flight delay measurements (suited for afterbody flows with larger plasma volumes), or more simple “transmissometer” techniques, where the plasma cutoff density along the line of sight may be determined by checking the limit frequency where electromagnetic waves start/stop being reflected back to the antenna. This technique is more suited for probing the shock layer in the spacecraft forebody, where the typically

small shock standoff distance disallows the determination of a plasma profile, and only the maximum electron density may be determined.

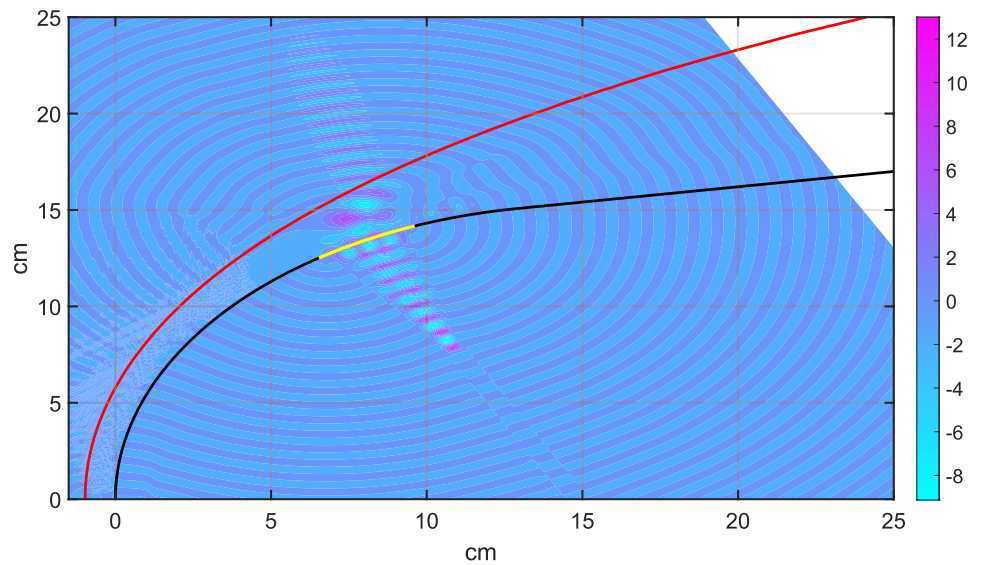
## 4 Conclusions

A detailed review of legacy in-flight (RAM-C II, OREX, HYFLEX, and ARD) and ground-test (plasma wind tunnels and shock tubes) microwave interferometry/reflectometry experiments is presented. Such diagnostic techniques have established a reasonable track record of providing absolute measurements of electron densities in specific locations of atmospheric entry plasmas. As such, they remain an invaluable technique for providing test-cases of reentry flows to serve as validation for numerical aerothermodynamic models, which can for example be attested by the popularity of the RAM-C test-case, which has been tackled by different teams in the past [14, 19–23, 68].

It is also true that such techniques have (a bit surprisingly) fallen out of flavor in the recent decades, and to the authors opinion, a renewed effort into developing a contemporary diagnostic of this kind, specifically tailored for atmospheric entry applications, would warrant to be undertaken. The specifications and requirements for such a state-of-the-art equipment may be derived from the experience gained from these past experiments.

One first task is the definition of the frequency bands which should be selected. It is fairly evident that there is no preferred band that may be pinpointed, owing to the very wide range of electron densities that may be found in atmospheric entry plasmas. Different entry speeds (for example orbital reentry speeds of about 6 km/s versus superorbital entry speeds around 11 km/s) will lead to different orders

**Fig. 15** REFMUL simulation for 35 GHz wave propagation in RAM-C II conditions. Spacecraft in black and shockwave in red. EM wave electric-field represented by the colorbar



of magnitude in the electron densities. Additionally, large discrepancies in the electron densities may be found even for a given entry speed, depending on whether one is probing the spacecraft forebody region near the shock (or carrying shock tube experiments in ground-test facilities), or whether one is probing the afterbody spacecraft plume (or simulating such plumes in freestream flows in supersonic plasma wind tunnels). As discussed in Sects. 2 and 3 electron densities range in between  $10^{16}$  el./m<sup>3</sup> and  $10^{22}$  el./m<sup>3</sup> (about 1 GHz–10 THz cutoff frequencies, respectively). This means that the choice frequency will be application-dependent, and a proper equipment should be highly modular in the band ranges it can probe, namely using appropriate frequency multiplier modules that may be switched on a case-by-case basis.

One possible design could be based on a signal generator with frequencies in the 2–18 GHz range (S, C, X, K<sub>u</sub> bands), coupled to frequency multipliers which would allow sampling frequencies up to 75–100 GHz (W band). The equipment should also provide enough flexibility so as to allow deploying it different configurations (reflectometer/interferometer/“transmissometer”), which specifically means enabling the hardware to be used in a monostatic (single antenna) configuration for reflectometry/“transmissometry” applications, or bistatic (two-antennas) configuration for interferometry applications. First testing campaigns should focus on “transmissometer” measurements, since although these can only provide info on the maximum electron density over the flight path of the electromagnetic waves, this info is already very useful for model validation purposes. Reflectometry diagnostics, based on the time-of-flight concept, are more demanding owing to the issues regarding spatial resolution and the fact that these diagnostics are better suited for larger plasma plumes. Accordingly, these measurement

techniques will only be deployed once interferometry measurement techniques will be well harnessed.

This paper also presents the RAM-C II experiment electron density, which was recreated through the SPARK CFD code, and then integrated in the REFMUL\* wave code to model the EM wave propagation in the electron field. The results show that the use of a reflectometer in the stagnation point region is very difficult since the plasma peak density is very high around  $10^{22}$  el./m<sup>3</sup> and the plasma is very compact, with reflectometry measurements being more adapted for the probing of afterbody flows. However, since typical plasma densities in the flow wake yield cutoff frequencies in the GHz range ( $\sim 10^{22}$  el./m<sup>3</sup>), the spatial resolution will be on a first basis equal to the signal wavelength. For 1 GHz frequency, this corresponds to 30 cm spatial resolution.<sup>2</sup> This might have proven sufficient for large spacecrafts like the Space Shuttle, with wave flows of several meters, however, this is not sufficient for smaller vehicles like the RAM-C II, which are increasingly the kind of vehicles which are operated contemporaneously. It is questionable on whether one would achieve good spatial resolutions using the time-of-flight reflectometry technique, making the “transmissometer” technique the most straightforward one to be deployed in in-flight experiments, although no information other than the maximum electron density over the line of sight would be retrieved in this case.

**Acknowledgements** All authors certify that they have no affiliations with or involvement in any organization or entity with any financial interest or non-financial interest in the subject matter or materials discussed in this manuscript. This work has been

<sup>2</sup> although other techniques may improve this spatial resolution, see Ref. [33].

supported by the Fundação Para a Ciência e Tecnologia, under Projects UIDB/50010/2020 and UIDP/50010/2020 and the grant PD/BD/114325/2016 (PD-F APPLAuSE).

**Funding** Open access funding provided by FCTIFCCN (b-on).

**Data availability** The data and information was retrieved from the aforementioned reference 33 - Seals, Joseph, et al. Microwave reflectometer ionization sensor. No. NASA-CR-191464. 1993.

**Open Access** This article is licensed under a Creative Commons Attribution 4.0 International License, which permits use, sharing, adaptation, distribution and reproduction in any medium or format, as long as you give appropriate credit to the original author(s) and the source, provide a link to the Creative Commons licence, and indicate if changes were made. The images or other third party material in this article are included in the article's Creative Commons licence, unless indicated otherwise in a credit line to the material. If material is not included in the article's Creative Commons licence and your intended use is not permitted by statutory regulation or exceeds the permitted use, you will need to obtain permission directly from the copyright holder. To view a copy of this licence, visit <http://creativecommons.org/licenses/by/4.0/>.

## References

- Hutchinson, I.H.: *Principles of Plasma Diagnostics* (Cambridge University Press, 2002). <https://www.xarg.org/ref/a/0521803896/>. Accessed May 2022
- Budden, K.G.: *Radio Waves in the Ionosphere* (Cambridge University Press, 2009). <https://www.xarg.org/ref/a/052111439X/>. Accessed May 2022
- Ginzburg, V.: *Propagation of Electromagnetic Waves in Plasma* (Gordon and Breach, 1962). <https://www.xarg.org/ref/a/0677200803/>. Accessed May 2022
- Simonet, F.: Measurement of electron density profile by microwave reflectometry on tokamaks. *Rev. Sci. Instrum.* **56**(5), 664 (1985). <https://doi.org/10.1063/1.1138200>
- Bottollier-Curtet, H., Ichtchenko, G.: Microwave reflectometry with the extraordinary mode on tokamaks: Determination of the electron density profile of Petula-B. *Rev. Sci. Instrum.* **58**(4), 539 (1987). <https://doi.org/10.1063/1.1139266>
- Hubbard, A.E., Costley, A.E., Gowers, C.W.: A simple fixed-frequency reflectometer for plasma density profile measurements on JET. *J. Phys. E* **20**(4), 423 (1987). <https://doi.org/10.1088/0022-3735/20/4/016>
- Luhmann, N.C., Bindslev, H., Park, H., Sánchez, J., Taylor, G., Yu, C.X.: Chapter 3: Microwave Diagnostics. *Fusion Science and Technology* **53**(2), 335 (2008). <https://doi.org/10.13182/fst08-a1675>
- Mazzucato, E.: Microwave reflectometry for magnetically confined plasmas. *Rev. Sci. Instrum.* **69**(6), 2201 (1998). <https://doi.org/10.1063/1.1149121>
- Estrada, T., Nagasaki, K., Blanco, E., Perez, G., Tribaldos, V.: Microwave Reflectometry Diagnostics: Present Day Systems and Challenges for Future Devices. *Plasma Fusion Res.* **7**, 2502055 (2012). <https://doi.org/10.1585/pfr.7.2502055>
- Bindslev, H.: Relativistic expressions for plasma cutoffs. *Plasma Phys. Controlled Fusion* **35**(9), 1093 (1993). <https://doi.org/10.1088/0741-3335/35/9/002>
- Bachynski, M.P.: Electromagnetic wave penetration of reentry plasma sheaths. *J. Res. Natl. Bureau Standards Sect. D-Radio Sci.* **69**(2), 147 (1965)
- da Silva, F., Heuraux, S., Hacquin, S., Manso, M.: Unidirectional transparent signal injection in finite-difference time-domain electromagnetic codes –application to reflectometry simulations. *J. Comput. Phys.* **203**(2), 467 (2005). <https://doi.org/10.1016/j.jcp.2004.09.002>
- da Silva, F., Heuraux, S., Ricardo, E., Silva, A., Ribeiro, T.: Modelling reflectometry diagnostics: finite-difference time-domain simulation of reflectometry in fusion plasmas. *J. Instrum.* **14**(08), C08003 (2019). <https://doi.org/10.1088/1748-0221/14/08/c08003>
- Loureiro, D.D.: High-temperature modeling of transport properties in hypersonic flows. Master's thesis, Instituto Superior Técnico, Universidade de Lisboa (2015)
- Hartunian, R.A., Stewart, G.E., Ferguson, S.D., Curtiss, T.J., Seibold, R.W., et al.: Causes and mitigation of radio frequency (rf) blackout during reentry of reusable launch vehicles. Aerospace Corporation, Tech. rep. (2007)
- Nina, D., Silva, C., Frassinetti, L., Gil, L., Hillesheim, J. et al.: in *46th European Physical Society Conference on Plasma Physics, EPS 2019, 8-12 July 2019, Milan, Italy* (European Physical Society (EPS), 2019)
- Jones, W.L., Cross, A.E.: *Electrostatic-probe measurements of plasma parameters for two reentry flight experiments at 25000 feet per second*, vol. 6617 (National Aeronautics and Space Administration, 1972)
- Grantham, W.L.: *Flight results of a 25000-foot-per-second reentry experiment using microwave reflectometers to measure plasma electron density and standoff distance*, vol. 6062 (National Aeronautics and Space Administration, 1970)
- Andrienko, D.: Non-equilibrium models for high temperature gas flows. Ph.D. thesis, Wright State University (2014)
- Farbar, E., Martin, A., Boyd, I., Kim, M.K.: in *42nd AIAA Thermophysics Conference* (American Institute of Aeronautics and Astronautics, 2011). <https://doi.org/10.2514/6.2011-3136>
- Soubrié, T.: Prise en compte de l'ionisation et du rayonnement dans la modélisation des écoulements de rentrée terrestre et martienne. Ph.D. thesis, ISAE-SUPAERO (2006). <http://www.theses.fr/2006ESAE0012>
- Walpot, L.: Development and application of a hypersonic flow solver. Ph.D. thesis, Delft University of Technology (2002)
- Josyula, E., Bailey, W.F.: Governing Equations for Weakly Ionized Plasma Flowfields of Aerospace Vehicles. *J. Spacecr. Rocket.* **40**(6), 845 (2003). <https://doi.org/10.2514/2.7036>
- Fujii, K., Imada, T., Kawato, H., Matsuda, S.: Concept Studies of HTV Derived Re-Entry System (2006). <https://doi.org/10.2514/6.2006-7935>. <https://arc.aiaa.org/doi/abs/10.2514/6.2006-7935>
- Shirouzu, M., Inouye, Y., Watanabe, S., Shigemi, M., Ueno, M., Yamamoto, Y., Ito, T.: in *34th AIAA Fluid Dynamics Conference and Exhibit* (American Institute of Aeronautics and Astronautics, 2004). <https://doi.org/10.2514/6.2004-2426>
- Gupta, R., Moss, J., Price, J.: in *31st Thermophysics Conference* (American Institute of Aeronautics and Astronautics, 1996). <https://doi.org/10.2514/6.1996-1859>
- Ito, T., Takaki, R., Teraoka, K.: Plasma electron density measurement around hypersonic flight experiment vehicle. *J. Spacecr. Rocket.* **36**(4), 573 (1999). <https://doi.org/10.2514/3.27202>
- The atmospheric reentry demonstrator (ard) - a flight experiment for technology qualification within the european manned space transportation programme (mstp). [https://www.esa.int/esapub/bulletin/bullet89\\_.htm](https://www.esa.int/esapub/bulletin/bullet89_.htm). Accessed: 2021-11-24
- Tran, P., Paulat, J., Boukhobza, P.: in *In Flight Experiments for Hypersonic Vehicle Development* (Educational Notes RTO-EN-AVT-130, 2007)
- Reynier, P., Evans, D.: in *39th Plasmadynamics and Lasers Conference* (American Institute of Aeronautics and Astronautics, 2008). <https://doi.org/10.2514/6.2008-3894>
- Reynier, P., Evans, D.: Postflight Analysis of Inflatable Reentry and Descent Technology Blackout During Earth Reentry. *J.*

- Spacecr. Rocket. **46**(4), 800 (2009). <https://doi.org/10.2514/1.41480>
32. Takahashi, Y., Nakasato, R., Oshima, N.: Analysis of Radio Frequency Blackout for a Blunt-Body Capsule in Atmospheric Reentry Missions. *Aerospace* **3**(1), 2 (2016). <https://doi.org/10.3390/aerospace3010002>
  33. Seals, J., Fordham, J.A., Pauley, R.G., Simonutti, M.D.: Microwave reflectometer ionization sensor. NASA Langley Research Center, CR **191464** (1993)
  34. Chikhaoui, A., Lino da Silva, M., Mota, S., Resendes, D.: Support during the MIPT Shock Tube Calibration. Tech. rep, European Space Agency (2008)
  35. Beck, J.: CFD validation in a CO<sub>2</sub> environment: synthesis report. Tech. rep., Fluid Gravity Report CR012/08., Emsworth, UK (2008)
  36. Reynier, P., Bugel, M., Smith, A.: Survey of European and major ISC facilities for supporting Mars and sample return mission aerothermodynamics and tests required for thermal protection system and dynamic stability. *Int. J. Aerosp. Eng.* **2011** (2011). <https://doi.org/10.1155/2011/937629>
  37. Anokhin, E.M.: Physical and chemical relaxation behind strong-shock waves in co-2-n2 mixtures. Ph.D. thesis, Moscow Institute of Physics and Technology (MIPT), Moscow, Russia (2005)
  38. Bugel, M., Reynier, P., Smith, A.: Survey of European and Major ISC Facilities for Supporting Mars and Sample Return Mission Aerothermodynamics and Tests Required for Thermal Protection System and Dynamic Stability. *Int. J. Aerospace Eng.* **2011**, 1 (2011). <https://doi.org/10.1155/2011/937629>
  39. Toujani, N., Alqaity, A.B.S., Farooq, A.: Electron density measurements in shock tube using microwave interferometry. *Rev. Sci. Instrum.* **90**(5), 054706 (2019). <https://doi.org/10.1063/1.5086854>
  40. Schneider, K.P., Park, C.: Shock tube study of ionization rates of NaCl-contaminated argon. *Phys. Fluids* **18**(8), 969 (1975). <https://doi.org/10.1063/1.861270>
  41. Gilchrist, B.E., Ohler, S.G., Gallimore, A.D.: Flexible microwave system to measure the electron number density and quantify the communications impact of electric thruster plasma plumes. *Rev. Sci. Instrum.* **68**(2), 1189 (1997). <https://doi.org/10.1063/1.1147882>
  42. Harwell, K.E., Jahn, R.G.: Initial Ionization Rates in Shock-Heated Argon, Krypton, and Xenon. *Phys. Fluids* **7**(2), 214 (1964). <https://doi.org/10.1063/1.1711135>
  43. Karasevich, Y.K.: Kinetics of chemical ionization in shock waves: I. Ionization kinetics in hydrocarbon oxidation. *Kinetics and Catalysis* **49**(5), 610 (2008). <https://doi.org/10.1134/s0023158408050029>
  44. Hofer, R., Haas, J., Gallimore, A.: in *39th AIAA/ASME/SAE/ASEE Joint Propulsion Conference and Exhibit* (American Institute of Aeronautics and Astronautics, 2003). <https://doi.org/10.2514/6.2003-4556>
  45. Eckman, R., Byrne, L., Gatsonis, N.A., Pencil, E.J.: Triple Langmuir Probe Measurements in the Plume of a Pulsed Plasma Thruster. *J. Propul. Power* **17**(4), 762 (2001). <https://doi.org/10.2514/2.5831>
  46. Matlock, T., Hargus, W., Larson, C., Nakles, M.: in *43rd AIAA/ASME/SAE/ASEE Joint Propulsion Conference & Exhibit* (American Institute of Aeronautics and Astronautics, 2007). <https://doi.org/10.2514/6.2007-5303>
  47. Ohler, S., Gilchrist, B., Gallimore, A.: in *31st Joint Propulsion Conference and Exhibit* (American Institute of Aeronautics and Astronautics, 1995). <https://doi.org/10.2514/6.1995-2931>
  48. Ohler, S., Gilchrist, B.E., Gallimore, A.: Microwave Plume Measurements of a Closed Drift Hall Thruster. *J. Propul. Power* **14**(6), 1016 (1998). <https://doi.org/10.2514/2.5367>
  49. Ohler, S.G., Gilchrist, B.E., Gallimore, A.D.: Nonintrusive electron number density measurements in the plume of a 1 kW arcjet using a modern microwave interferometer. *IEEE Trans. Plasma Sci.* **23**(3), 428 (1995). <https://doi.org/10.1109/27.402337>
  50. Cappelli, M.A., Gascon, N., Hargus, W.A.: Millimetre wave plasma interferometry in the near field of a Hall plasma accelerator. *J. Phys. D Appl. Phys.* **39**(21), 4582 (2006). <https://doi.org/10.1088/0022-3727/39/21/013>
  51. Reed, G., Hargus, W., Cappelli, M.: *Microwave Interferometry (90 GHz) for Hall Thruster Plume Density Characterization* (2005). <https://doi.org/10.2514/6.2005-4399>
  52. Kuwabara, N., Chono, M., Yamamoto, N., Kuwahara, D.: in *36th International Electric Propulsion Conference, Vienna, Austria, IEPC-2019-665* (2019)
  53. Kuwabara, N., Chono, M., Yamamoto, N., Kuwahara, D.: Electron Density Measurement Inside a Hall Thruster Using Microwave Interferometry. *J. Propul. Power* **37**(3), 491 (2021)
  54. Mota, S., Resendes, D.P., Cupido, L.: in *Proceedings of the 31st International Electrical Propulsion Conference* (American Institute of Aeronautics and Astronautics, 2009)
  55. Silva, A.G., da Silva, F., Heuraux, S., Gonçalves, B.: First assessment of microwave diagnostics for DEMO. *Fusion Engineering and Design* **96–97**, 948 (2015). <https://doi.org/10.1016/j.fusengdes.2015.06.137>. <https://www.sciencedirect.com/science/article/pii/S092037961530168X>. Proceedings of the 28th Symposium On Fusion Technology (SOFT-28). Accessed June 2022
  56. Cruz, N., Batista, A.J.N., Cardoso, J.M., Carvalho, B.B., Carvalho, P.F., Combo, A., Correia, M., Fernandes, A., Pereira, R.C., Rodrigues, A.P., Santos, B., Sousa, J., Gonçalves, B.: Advanced high-performance processing tools for diagnostics and control in fusion devices. *Fusion Engineering and Design* **170**, 112529 (2021). <https://doi.org/10.1016/j.fusengdes.2021.112529>. <http://www.sciencedirect.com/science/article/pii/S0920379621003057>. Accessed June 2022
  57. Lopez, B., da Silva, M.L.: SPARK: a Software Package for Aerodynamics, Radiation and Kinetics. 46th AIAA Thermophysics Conference (2016). <https://doi.org/10.2514/6.2016-4025>
  58. Park, C., Jaffe, R.L., Partridge, H.: Chemical-Kinetic Parameters of Hyperbolic Earth Entry. *J. Thermophys. Heat Transfer* **15**(1), 76 (2001). <https://doi.org/10.2514/2.6582>
  59. Wilke, C.R.: A Viscosity Equation for Gas Mixtures. *J. Chem. Phys.* **18**(4), 517 (1950). <https://doi.org/10.1063/1.1747673>
  60. Gupta, R.N., Yos, J.M., Thompson, R.A., Lee, K.P.: A review of reaction rates and thermodynamic and transport properties for an 11-species air model for chemical and thermal nonequilibrium calculations to 30000 K. Tech. Rep. RP 1232, NASA (1990)
  61. Silva, F.D., Heuraux, S., Ribeiro, T., Aguiam, D.: in *42nd EPS Conference on Plasma Physics* (European Physical Society, 2015)
  62. da Silva, F., Ferreira, J., De Masi, G., Heuraux, S., Ricardo, E., Ribeiro, T., Tudisco, O., Cavazzana, R., D'arcangelo, O., Silva, A.: A first full wave simulation assessment of reflectometry for DTT. *J. Instrum.* **14**(08), C08011 (2019)
  63. da Silva, F., Heuraux, S., Ricardo, E., Silva, A., Ribeiro, T.: Benchmarking 2D against 3D FDTD codes in the assessment of reflectometry performance in fusion devices. *J. Instrum.* **14**(08), C08004 (2019)
  64. Vicente, J., da Silva, F., Heuraux, S., Conway, G.D., Silva, C., Ribeiro, T.: Turbulence level effects on conventional reflectometry using 2D full-wave simulations. *Rev. Sci. Instrum.* **89**(10), 10H110 (2018). <https://doi.org/10.1063/1.5038756>
  65. Vicente, J., Silva, F.D., Ribeiro, T., Heuraux, S., Conway, G., Scott, B., Guimarães, L., Gil, L., Seliunin, E., Manz, P., Santos, J., Silva, A., Silva, C.: Synthetic conventional reflectometry probing of edge and scrape-off layer plasma turbulence. *J. Instrum.* **14**(10), C10043 (2019). <https://doi.org/10.1088/1748-0221/14/10/c10043>
  66. Vicente, J., da Silva, F., Hoelzl, M., Conway, G., Heuraux, S.: A simulation chain for reflectometry and non-linear MHD: type-I ELM case. *J. Instrum.* **16**(12), C12024 (2021)

67. Berenger, J.: A perfectly matched layer for the absorption of electromagnetic waves. *J. Comput. Phys.* **114**(2), 185 (1994). <https://doi.org/10.1006/jcph.1994.1159>
68. Alkandry, H., Boyd, I.D., Martin, A.: in 51st AIAA Aerospace Sciences Meeting including the New Horizons Forum and Aerospace Exposition (Grapevine, Texas **2013–0303**, 1–18 (2013)

**Publisher's Note** Springer Nature remains neutral with regard to jurisdictional claims in published maps and institutional affiliations.